

RESEARCH

Open Access



# Probiotic nanocomposite materials with excellent resistance, inflammatory targeting, and multiple efficacies for enhanced treatment of colitis in mice

Yuwen Huang<sup>1†</sup>, Hongting Cai<sup>1†</sup>, Huipeng Liu<sup>1†</sup>, Lixiang Wang<sup>1†</sup>, Guangfu Feng<sup>1\*</sup>, Zizi Ding<sup>1</sup>, Yanquan Fei<sup>1</sup>, Aike Li<sup>2\*</sup> and Jun Fang<sup>1\*</sup>

## Abstract

The occurrence of inflammatory bowel disease (IBD) is relevant to impaired intestinal mucosal barrier and disordered gut microbiota, subsequently leading to excessive production of reactive oxygen species (ROS) and elevated levels of inflammatory factors. Traditional therapies focus on inhibiting inflammation, but the vast majority involve non-targeted systemic administration, whose long-term use may result in potential side effects. Oral microbial therapy has exhibited great application prospects currently in IBD treatment; however, its progress has been slowed by issues with deficient bioavailability, poor targeting of colitis, and low therapeutic efficacy. Consequently, it is exceedingly desirable to develop a strategy by which probiotics can be endowed with additional anti-inflammatory and antioxidant properties, as well as enhanced targeting of the inflamed intestine. Herein, we present an innovative therapeutic strategy for encapsulating probiotic *Bacillus coagulans* spores with rosmarinic acid (RA) and silk fibroin (SF). Probiotics in spore morphology possessed strong gastrointestinal environmental resistance; RA alleviated oxidative damage by scavenging ROS and inhibited inflammatory responses; SF assisted probiotics release and colonize in the inflamed intestine. We demonstrated the therapeutic efficacy of probiotic composite materials in a colitis mouse model, which significantly alleviated a series of colitis symptoms, inhibited inflammatory cytokine storms, restored the balance of the gut microbiota, and downregulated inflammation-related signaling pathways. We are optimistic that the utilization of therapeutic nanocoating to modify probiotics will open up novel avenues for future microbial therapy targeting IBD.

<sup>†</sup>Yuwen Huang, Hongting Cai, Huipeng Liu and Lixiang Wang contributed equally to this work.

\*Correspondence:

Guangfu Feng  
GuangfuFeng@hunau.edu.cn  
Aike Li  
lak@AGS.AC.CN  
Jun Fang  
fangjun1973@hunau.edu.cn

Full list of author information is available at the end of the article



© The Author(s) 2025. **Open Access** This article is licensed under a Creative Commons Attribution-NonCommercial-NoDerivatives 4.0 International License, which permits any non-commercial use, sharing, distribution and reproduction in any medium or format, as long as you give appropriate credit to the original author(s) and the source, provide a link to the Creative Commons licence, and indicate if you modified the licensed material. You do not have permission under this licence to share adapted material derived from this article or parts of it. The images or other third party material in this article are included in the article's Creative Commons licence, unless indicated otherwise in a credit line to the material. If material is not included in the article's Creative Commons licence and your intended use is not permitted by statutory regulation or exceeds the permitted use, you will need to obtain permission directly from the copyright holder. To view a copy of this licence, visit <http://creativecommons.org/licenses/by-nc-nd/4.0/>.

**Keywords** Probiotic composite materials, Inflammatory bowel disease, *Bacillus coagulans*, Rosmarinic acid, Silk fibroin, Reactive oxygen species, Gut microbiota

## Introduction

Inflammatory bowel disease (IBD), a chronic inflammatory disease occurring in the gastrointestinal tract, consists of ulcerative colitis (UC) and Crohn's disease (CD), and may further induce more severe and fatal colorectal cancer [1, 2]. Despite the complex pathogenesis, emerging evidence indicates that IBD may be associated with impaired intestinal mucosal barrier function and disordered gut microbiota, subsequently leading to excessive production of reactive oxygen species (ROS) and elevated levels of inflammatory factors [3–5]. Presently, the majority of clinical treatment drugs for IBD, including 5-aminosalicylic acid (5-ASA), corticosteroids, immunosuppressants, and antibiotics, focus on alleviating symptoms linked to this disease through the suppression of intestinal inflammation [6–8]. While these medications do exhibit certain therapeutic effects, their long-term use may result in potential systemic side effects due to their lack of targeting [9, 10]. Moreover, they generally target a single IBD's trigger and are incapable of addressing critical concerns like excessive production of ROS and imbalance of gut microbiota concurrently [5, 11]. Therefore, novel therapy strategies are required to simultaneously target multiple triggers of IBD and reduce systemic side effects.

Oral administration of probiotics, a promising IBD therapy, can actively regulate the balance of gut microbiota and promote intestinal mucosal repair [12–15]. However, the efficacy of this therapy has been constrained by the harsh gastrointestinal environment, including gastric acid and digestive enzymes [16–18]. To improve the oral bioavailability of probiotics, various encapsulation and intestinal delivery techniques have been investigated [19–21]. Despite the fact that these methods possess the advantages of stabilizing probiotics and facilitating their delivery, advancements in science and technology have elevated standards for their biocompatibility, adhesion capability, responsive release capability, cost-effectiveness, and user-friendliness. Furthermore, natural probiotics are frequently insufficient to treat diseases when used alone as therapeutic ingredients. Therefore, strategies that confer additional antioxidant and anti-inflammatory properties to probiotics while improving their gastrointestinal resistance are highly desirable [11, 22–25].

*Bacillus coagulans* (BC), a “generally recognized as safe” lactic acid bacteria (LAB) approved by the US Food and Drug Administration (FDA), can produce a variety of beneficial metabolites such as lactic acid, thereby regulating gut microbiota and alleviating intestinal

inflammation [26–28]. Spores, as a dormant body of bacteria, are wrapped in a thick hydrophobic protein shell, which can resist harsh environments including gastric acid and high temperatures [29–31]. Additionally, BC spores can germinate into probiotics in the intestinal microenvironment in vivo, and then BC will colonize the intestine [32, 33]. Compared with other probiotics, these properties of BC spores improve their bioavailability in the gut, in turn enhancing their therapeutic effects. Interestingly, probiotic spores will consume free oxygen in the process of germination and reproduction after entering the intestine, which is conducive to the growth of anaerobic probiotics while squeezing the living space of aerobic pathogenic bacteria, thus regulating the intestinal microecological balance [34]. Rosmarinic acid (RA), a natural anti-inflammatory and antioxidant molecule, has the ability to reduce oxidative damage via scavenging free radicals in the body and inhibit the release of inflammatory mediators and the occurrence of inflammatory reactions [35–38]. Silk fibroin (SF) has excellent mechanical properties, biocompatibility, and biodegradability, thereby possessing broad application prospects in the biomedical field [39–41]. The surface of colonic epithelial cells and macrophages in the inflamed colon tissue highly expresses integrin receptors, which can recognize Arg-Gly-Asp (RGD) tripeptide, while SF from tussah silkworms just contains abundant RGD tripeptide [42–44]. Utilizing this property could potentially enhance targeting for colitis.

Cell surface modification, including chemical coupling and physical encapsulation, has been used to introduce some exogenous functions that cannot be achieved naturally [45, 46]. Compared with capsule packaging, single-encapsulated probiotics typically exhibit extraordinary bioavailability, controlled release characteristics, and therapeutic efficacy [20, 47]. To improve the ROS scavenging and anti-inflammatory abilities of probiotics, as well as their targeting ability towards the inflamed intestine, here, we describe a novel delivery strategy for encapsulating BC spores with RA and SF in combination to synergistically enhance their IBD therapeutic effects (Fig. 1). Briefly, RA was covalently bound to the surface of BC spores; SF shifted from a random coiled conformation to a  $\beta$ -sheet conformation, thereby self-assembling onto the bacterial surface [48]. The side effects of the preparation process and the formed nanocoating on bacterial viability could be ignored due to avoiding the use of organic solvents and other chemical reagents. The in vitro results showed that RA enhanced the ROS/RNS scavenging abilities of probiotic spores, while the combined use

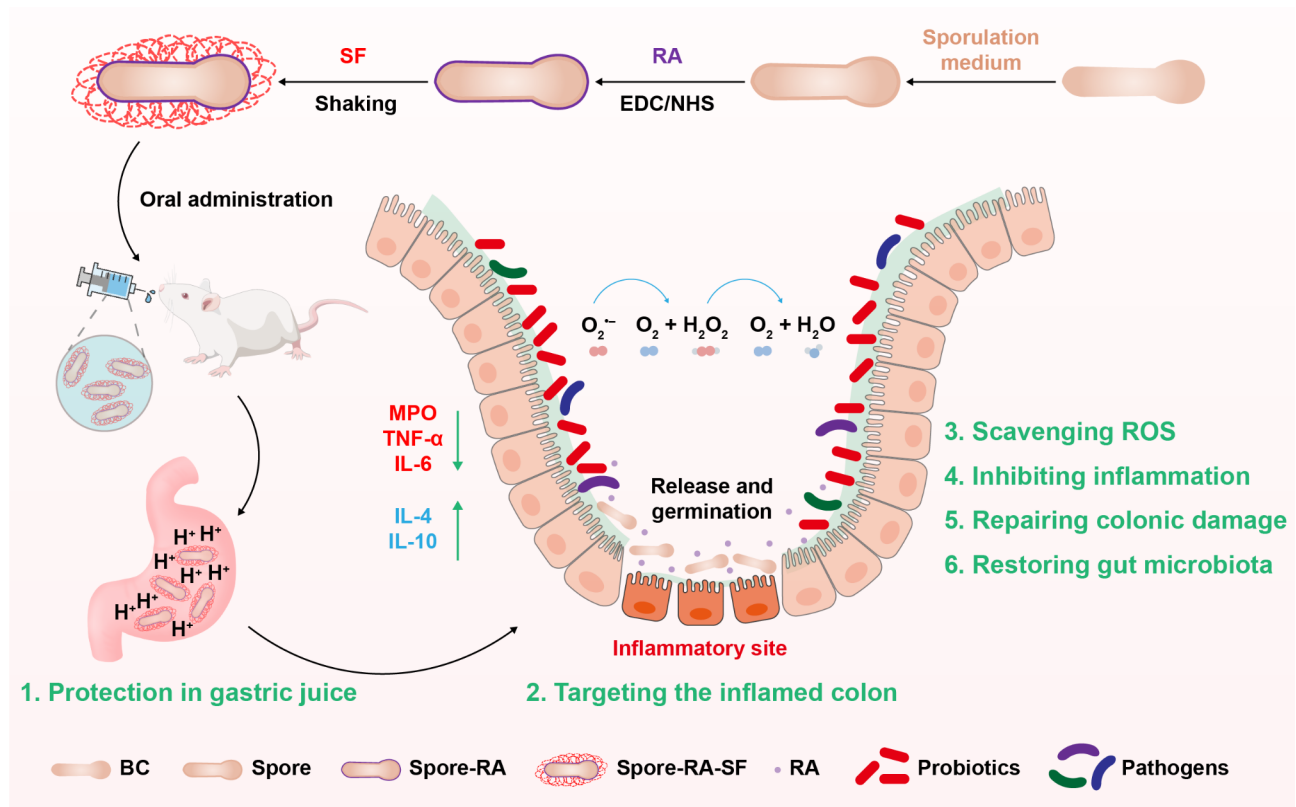


**Fig. 1** Strategy of RA-SF-encapsulated spores (Spore-RA-SF) for IBD treatment. BC spores were encapsulated with RA and SF in combination to enhance their ROS/RNS scavenging activities and targeting ability towards the inflamed intestine. Spore-RA-SF was orally administered to the colitis mice, and SF could protect the ROS/RNS scavenging activities of RA after passing through gastric juice. Spore-RA-SF alleviated colitis in mice by scavenging ROS, inhibiting inflammation, repairing colonic damage, and restoring gut microbiota

of SF protected these functions under simulated gastrointestinal environments. Mouse experiments demonstrated that our encapsulation strategy could enhance targeting ability in the inflamed intestine of probiotic spores. Moreover, the probiotic composite materials (Spore-RA-SF) did not induce any adverse effects on mice. In the mouse model of acute colitis induced by dextran sulfate sodium (DSS), RA-SF nanocoating significantly improved the therapeutic efficacy of BC spores. Specifically, weight loss, increased disease activity index (DAI), and colon shortening and lesions were remarkably alleviated in mice. The rising myeloperoxidase (MPO) activity and inflammatory factor storms in colon tissue were also significantly inhibited. Furthermore, gut microbiome and colon transcriptome analysis revealed that the disturbed gut microbiota of colitis mice restored balance, and inflammation-related signaling pathways such as the PI3K–Akt signaling pathway were inhibited. In view of the greatly enhanced oral bioavailability and therapeutic efficacy, we expect that the strategy of modifying probiotics with therapeutic nanocoating will likely serve as a general strategy for the preparation of advanced microbial agents and promote the clinical translation of probiotic therapy for IBD.

## Results and discussion

### Preparation and characterization of Spore-RA-SF

BC, the probiotic approved by the FDA, was selected in this work as its dormant spores are surrounded by a thick hydrophobic protein shell that can resist harsh environments such as gastric acid [32]. To endow BC spores with additional ROS/RNS scavenging and anti-inflammatory abilities, we chose the natural anti-inflammatory and antioxidant molecule RA to covalently bind to their surface. Furthermore, the natural protein SF extracted from tussah silkworms has excellent biocompatibility and biodegradability and has the ability to bind with inflammatory colonic epithelium [44]. It was thus used for the delivery of Spore-RA to enhance the bioavailability of probiotic composite materials. The preparation process of Spore-RA-SF is shown in Fig. 2a, and we speculate that the combined encapsulation of RA and SF could synergistically enhance the therapeutic effect of probiotic BC on IBD.

To verify the successful modification of RA and SF, we conducted a series of characterizations on probiotic composite materials. The scanning electron microscopy (SEM) images showed that the loading of RA and SF increased the volume of spores, and the surface of

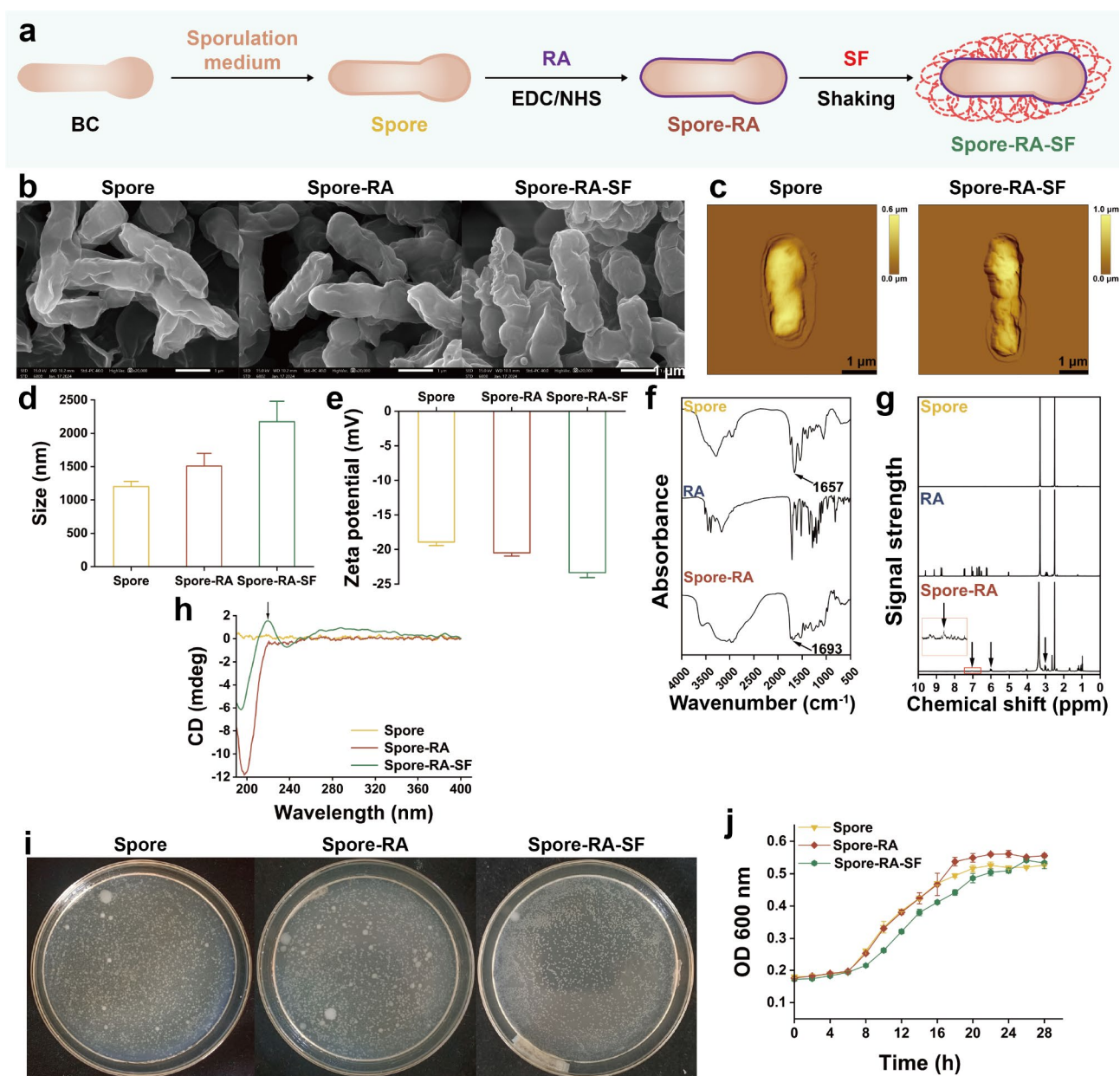


**Fig. 2** Preparation and characterization of Spore-RA-SF. **(a)** Schematic diagram of the preparation process of Spore-RA-SF. BC spores were modified with RA and then encapsulated with SF. **(b)** Representative SEM images of Spore, Spore-RA, and Spore-RA-SF. Scale bar: 1  $\mu\text{m}$ . **(c)** Representative AFM images of Spore and Spore-RA-SF. Scale bar: 1  $\mu\text{m}$ . **(d)** Sizes and **(e)** zeta potential of Spore, Spore-RA, and Spore-RA-SF. **(f)** FT-IR and **(g)**  $^1\text{H}$  NMR spectra of Spore and Spore-RA. **(h)** CD spectra of Spore, Spore-RA, and Spore-RA-SF. **(i)** Bacterial colonies of Spore, Spore-RA, and Spore-RA-SF grown on agar plates. **(j)** Growth curves of Spore, Spore-RA, and Spore-RA-SF cultured in MRS medium. Data were presented as the mean  $\pm$  standard deviation ( $n=3$  biologically independent samples). Statistical analysis was evaluated with two-tailed Student's  $t$  tests (\* $P < 0.05$ , \*\* $P < 0.01$ , \*\*\* $P < 0.001$ , \*\*\*\* $P < 0.0001$ )

Spore-RA-SF was coated with a thick layer (Fig. 2b). The changes in the content of different elements could reflect the loading of RA and SF: the increase in carbon content in Spore-RA may be attributed to the high carbon content of RA; the increase in sulfur content in Spore-RA-SF may be attributed to the sulfur in SF (Supplementary Fig. 1). Atomic force microscopy (AFM) images further revealed the surface microstructure of SF-coated spores: their surface became rough and thickness significantly

increased (Fig. 2c). To evaluate the loading rate of RA and the thickness of the RA-SF nanocoating, we measured the UV absorption at 330 nm of the solution before (+) and after (-) RA loading, and the nanoparticle sizes of different materials. According to Supplementary Fig. 2, the loading rate of RA was approximately 24.7%. The average thickness of the RA-SF nanocoating was about 487 nm (Fig. 2d). The encapsulation of the negatively charged SF reduced the zeta potential of spores from

-18.9 mV to -23.4 mV (Fig. 2e). Moreover, the chemical structures of Spore-RA were characterized by Fourier transform infrared (FT-IR) spectroscopy and  $^1\text{H}$  nuclear magnetic resonance (NMR) spectroscopy. As shown in Fig. 2f, the covalent binding of RA via amide bonds caused the stretching vibration peak of Spore to shift from  $1657\text{ cm}^{-1}$  to  $1693\text{ cm}^{-1}$ . In the  $^1\text{H}$  NMR spectra of Spore-RA, the peaks of aromatic hydrogen, vinyl hydrogen, and ether-bonded hydrogen belonging to RA were observed at 7, 6, and 3 ppm, respectively (Fig. 2g). The circular dichroism (CD) spectrum indicated the SF wrapped on Spore-RA presented the characteristic peak (217 nm) of the  $\beta$ -sheet (Fig. 2h). Altogether, the above results demonstrated the successful encapsulation of RA and SF.

To evaluate the retention time of the RA-SF coating on spore surfaces, we labeled Spore-RA-SF with fluorescein isothiocyanate (FITC). After incubating in ultrapure water or MRS medium for a period of time, the fluorescence on spore surfaces was observed using a fluorescence microscope. The Spore-RA-SF in ultrapure water still showed significant fluorescence after 72 h of storage, with only a slight difference compared to 0 h (Supplementary Fig. 3). However, the Spore-RA-SF incubated in MRS medium showed reduced fluorescence after 6 h and almost lost fluorescence after 24 h. The above results indicated that the RA-SF coating could be retained on spore surfaces for at least 3 days, while the germination and growth of spores caused the RA-SF coating to detach. Additionally, the number and morphology of Spore, Spore-RA, and Spore-RA-SF bacterial colonies grown on agar plates, along with their growth curves cultured in MRS medium, showed that the encapsulation of RA and SF had no significant effect on the growth of spores (Fig. 2i, j). We can conduct further in vitro functional studies on Spore-RA-SF.

#### In vitro functional evaluation of Spore-RA-SF

To verify the inhibitory effect of spores on the growth of harmful bacteria in vitro, we co-incubated *Escherichia coli* (*E. coli*) DH5 $\alpha$  with Spore, Spore-RA, or Spore-RA-SF in LB medium, and then the co-incubated medium was equally diluted and coated on Enterobacteriaceae selective MacConkey agar plates. The results showed that Spore, Spore-RA, and Spore-RA-SF all had significantly inhibitory effects on the growth of *E. coli* DH5 $\alpha$  (Fig. 3a and Supplementar Fig. 4). We speculated that this inhibition may originate from the hypoxia effect produced by the germination and propagation of BC spores [34]; therefore, we further detected the oxygen consumption of Spore and Spore-RA-SF in the medium. As shown in Fig. 3b, spores began to germinate rapidly and consumed dissolved oxygen significantly around 12 h, whereas RA-SF encapsulation had a negligible delay effect on

spore germination and did not affect their consumption of dissolved oxygen.

Excessive ROS/RNS in the inflammatory region will lead to intestinal tissue damage and the destruction of key intestinal proteins, ultimately damaging the integrity of the intestinal barrier and exacerbating the development of IBD [49]. In consideration of this, we conducted an in vitro assessment of the ROS/RNS scavenging capacity of probiotic composite materials (Fig. 3c). Firstly, the representative small molecule ROS superoxide anion radical ( $\text{O}_2^{\cdot-}$ ) and hydrogen peroxide ( $\text{H}_2\text{O}_2$ ) in IBD were tested [50, 51]. The superoxide dismutase (SOD)-like activity of  $\text{O}_2^{\cdot-}$  elimination was studied by the nitroblue tetrazolium (NBT) method. As shown in Fig. 3d, by measuring the absorbance peak intensity at 560 nm, it was found that the  $\text{O}_2^{\cdot-}$  scavenging ratios of both the Spore-RA group and the Spore-RA-SF group were significantly higher compared with the Spore group. We studied the catalase (CAT)-like activity of  $\text{H}_2\text{O}_2$  dismutation by the ammonium molybdate method. Consistent with the above results, the encapsulation of RA or RA-SF significantly improved the  $\text{H}_2\text{O}_2$  scavenging efficiency of spores (Fig. 3e). In addition, we selected typical RNS 2,2'-azino-bis(3-ethyl-benzothiazoline-6-sulfonic acid) diammonium salt (ABTS) and 1,1-diphenyl-2-picrylhydrazyl (DPPH), as well as ROS 2-phenyl-4,4,5,5-tetramethylimidazole-3-oxide-1-oxyl (PTIO) [52]. When ABTS is oxidized by  $\text{K}_2\text{S}_2\text{O}_8$  to the stable radical  $\text{ABTS}^{\cdot+}$ , the resulting blue-green solution has a characteristic absorption peak at 734 nm. By monitoring and quantifying the decolorization of the solution, it can be found that Spore-RA and Spore-RA-SF had significantly stronger  $\text{ABTS}^{\cdot+}$  scavenging abilities than Spore (Fig. 3f). DPPH $\cdot$  is a stable RNS, whose ethanol solution is purple with a characteristic absorption peak at 519 nm. As shown in Fig. 3g, the loading of RA significantly improved the DPPH $\cdot$  scavenging activity of spores, and the DPPH $\cdot$  scavenging ratio of Spore-RA-SF was also higher than that of Spore. PTIO $\cdot$  is a stable ROS with a blue-purple color in solution and an absorption peak at 557 nm. We found that both Spore-RA and Spore-RA-SF had remarkably higher PTIO $\cdot$  scavenging ratios than Spore by observing and measuring the decolorization of the solution (Fig. 3h). In conclusion, our modification of spores endowed them with excellent ROS/RNS scavenging abilities in vitro.

The harsh environment of the gastrointestinal tract, including gastric acid and digestive enzymes, tests orally administered probiotics before they colonize the gut [16, 17]. Therefore, we prepared simulated gastric fluid (SGF, pH 2.0) containing pepsin, simulated intestinal fluid (SIF, pH 6.8) containing trypsin, and simulated colonic fluid (SCE, pH 7.8) to study the resistance of Spore-RA and Spore-RA-SF in the simulated gastrointestinal environment. Firstly, we evaluated the survival

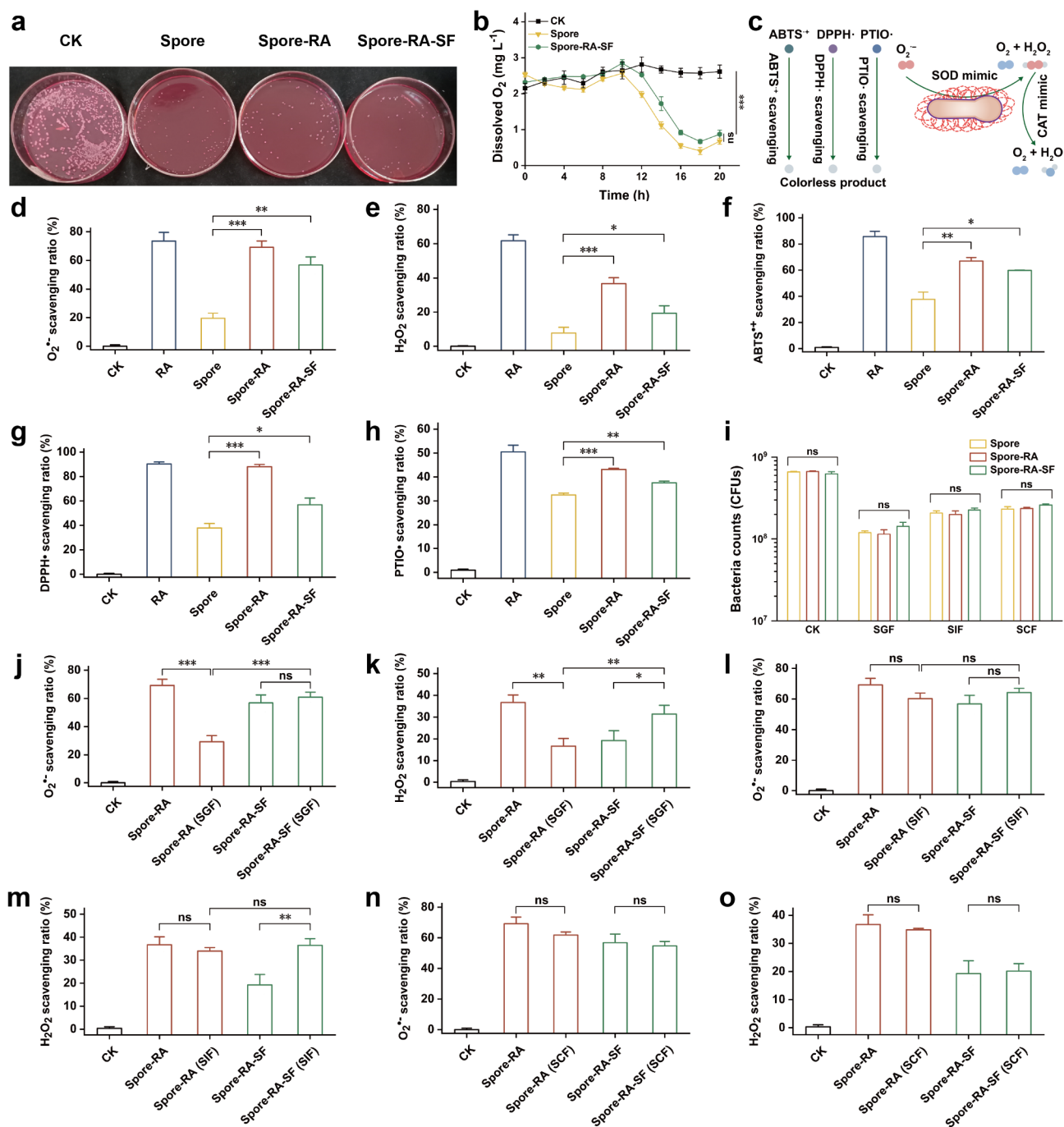


**Fig. 3** In vitro functional evaluation of Spore-RA-SF. **(a)** Inhibitory effects of Spore, Spore-RA, and Spore-RA-SF on the growth of *E. coli* DH5α (200 μL). **(b)** Changes in dissolved oxygen content over time in spore germination medium. **(c)** Schematic diagram of RA-modified spores scavenging ROS/RNS. **(d-h)** O<sub>2</sub><sup>-</sup>, H<sub>2</sub>O<sub>2</sub>, ABTS<sup>+</sup>, DPPH<sup>•</sup>, and PTIO<sup>•</sup> scavenging ratios in different groups. **(i)** Survival of Spore, Spore-RA, and Spore-RA-SF following exposure to SGF, SIF, or SCF for 1 h. **(j)** O<sub>2</sub><sup>-</sup> and **(k)** H<sub>2</sub>O<sub>2</sub> scavenging ratios after SGF incubation in different groups. **(l)** O<sub>2</sub><sup>-</sup> and **(m)** H<sub>2</sub>O<sub>2</sub> scavenging ratios after SIF incubation in different groups. **(n)** O<sub>2</sub><sup>-</sup> and **(o)** H<sub>2</sub>O<sub>2</sub> scavenging ratios after SCF incubation in different groups. CK: control check. Data were presented as the mean ± standard deviation (*n* = 3 biologically independent samples). Statistical analysis was evaluated with two-tailed Student's *t* tests (\**P* < 0.05, \*\**P* < 0.01, \*\*\**P* < 0.001, \*\*\*\**P* < 0.0001)

of Spore, Spore-RA, and Spore-RA-SF after incubation in different simulated gastrointestinal fluids for 1 h. The results showed that all treatment groups maintained high survival rates, even in SGF (Fig. 3i). Meanwhile,

no significant difference was found in the survival rates of Spore, Spore-RA, and Spore-RA-SF in different simulated gastrointestinal fluids. These results indicated that Spore's modification had no remarkable effect on

its excellent gastrointestinal environmental resistance. Secondly, the ROS/RNS scavenging efficiency of them after SGF, SIF, or SCF treatment was assessed [53]. As shown in Fig. 3j, k and Supplementary Fig. 5, the ROS/RNS scavenging ratios of Spore-RA after SGF treatment were significantly reduced. Surprisingly, the combined encapsulation of SF protected the ROS/RNS scavenging abilities of Spore-RA. There was no significant difference in the scavenging activities of  $O_2^{\cdot-}$ ,  $H_2O_2$ , and  $PTIO\cdot$  between Spore-RA and Spore-RA-SF after SIF treatment (Fig. 3l, m and Supplementary Fig. 6), while the scavenging abilities of  $ABTS^{+\cdot}$  and  $DPPH\cdot$  of Spore-RA-SF were remarkably excellent (Supplementary Fig. 6). After SCF treatment, no significant change was found in the  $O_2^{\cdot-}$  and  $H_2O_2$  scavenging abilities of Spore-RA and Spore-RA-SF (Fig. 3n, o). Unlike the Spore-RA group, where the scavenging activities of  $ABTS^{+\cdot}$ ,  $DPPH\cdot$ , and  $PTIO\cdot$  were significantly reduced, the Spore-RA-SF group showed no remarkable change in the scavenging activities of these three ROS/RNS after SCF treatment (Supplementary Fig. 7). The above results showed that the combined encapsulation of RA and SF could maintain the resistance of spores to the gastrointestinal environment and protect the ROS/RNS scavenging abilities of Spore-RA after passing through the gastrointestinal tract. Additionally, we speculated that the increases in ROS/RNS scavenging ratios in the Spore-RA-SF group after incubation with SGF or SIF could be attributed to the shielding of RA's activities by SF encapsulation and the degradation of SF by digestive enzymes.

#### **In vivo targeting and biosafety of Spore-RA-SF**

To test the in vivo targeting ability of probiotic composite materials, we orally administered FITC-labeled Spore or Spore-RA-SF to healthy mice or DSS-induced colitis mice [11, 17, 54]. Colitis was induced by adding 3% (w/v) DSS to the drinking water of mice for 7 consecutive days, and then the mice were sacrificed at 2, 4, 8, 12, or 24 h after oral administration of Spore or Spore-RA-SF, and the intestines were collected for in vivo imaging system (IVIS) imaging (Fig. 4a). As shown in Fig. 4b, c, the total fluorescence intensities of mouse colons in the Spore + 3% DSS group and the Spore-RA-SF + Water group reached the maximum at 4 h, and the total fluorescence intensities of mouse colons in the Spore-RA-SF + 3% DSS group at 8 and 12 h were significantly higher than those in the other two groups. These results validated the hypothesis that our probiotic composite materials exhibited targeting ability towards the inflamed colon.

Before treating mouse colitis, we evaluated the biosafety of Spore-RA-SF (Fig. 4d) [16, 23]. As shown in Fig. 4e, no reduction in body weight was observed in healthy mice that were orally administered PBS or Spore-RA-SF, and the trend of body weight change was

consistent in both groups. Furthermore, hematoxylin and eosin (H&E) staining images of major organs (heart, liver, spleen, lung, and kidney) and hemolysis test results indicated that Spore-RA-SF had no toxic side effects (Fig. 4f, g).

#### **Therapeutic efficacy of Spore-RA-SF against mouse colitis**

Next, we evaluated the therapeutic efficacy of Spore-RA-SF in the DSS-induced colitis mouse model (Fig. 5a). Colitis was induced by adding 3% (w/v) DSS to the drinking water of mice for 7 consecutive days, and then the colitis mice were treated with various oral formulas (RA, Spore, Spore-RA, or Spore-RA-SF) on days 0, 2, 4, 6, and 8. The mice were sacrificed on day 10, and the colons were collected to evaluate the efficacy of various therapeutic formulas (Fig. 5b). Compared with the untreated DSS group, the administration of Spore-RA-SF significantly alleviated a series of symptoms of DSS-induced mouse colitis, including loss of body weight, increase in DAI, and shortening of colon length [23], while the therapeutic efficacy of Spore or Spore-RA was obviously inferior to that of Spore-RA-SF (Fig. 5c-e and Supplementary Fig. 8). Moreover, H&E staining images, as well as colonic damage scores, showed that among all treatment groups, Spore-RA-SF treatment could most effectively reverse the pathological damage of colonic epithelium in colitis mice (Fig. 5f, g). Immunohistochemical staining images further illustrated that Spore-RA-SF could effectively reduce MPO activity in colon tissue and alleviate oxidative stress (Fig. 5h). The immunofluorescence staining for occludin in colon tissue confirmed that Spore-RA and Spore-RA-SF had excellent restoration effects on the intestinal barrier in colitis mice (Fig. 5i). As shown in Fig. 5j, k, the levels of pro-inflammatory factors tumor necrosis factor- $\alpha$  (TNF- $\alpha$ ) and interleukin-6 (IL-6) were significantly increased in the colon of untreated DSS mice, while Spore-RA-SF treatment remarkably reduced the levels of these inflammatory factors. Meanwhile, the expression levels of anti-inflammatory factors IL-4 and IL-10 were significantly increased in the Spore-RA-SF treatment group (Fig. 5l, m). To sum up, our probiotic composite materials could remarkably alleviate DSS-induced colitis in mice.

#### **Modulation of gut microbiota by Spore-RA-SF**

Dysbiosis of the gut microbiota, including aberrant proliferation of Enterobacteriaceae and loss of beneficial bacterial taxa, is currently found to be closely associated with the development of IBD [4, 55, 56]. To test whether Spore-RA-SF could relieve gut microbiota dysbiosis in colitis, we analyzed the colonic contents of mice in different treatment groups via 16 S ribosomal RNA (16 S rRNA) sequencing to study their gut microbiota changes. As the number of sequences sampled increased, the

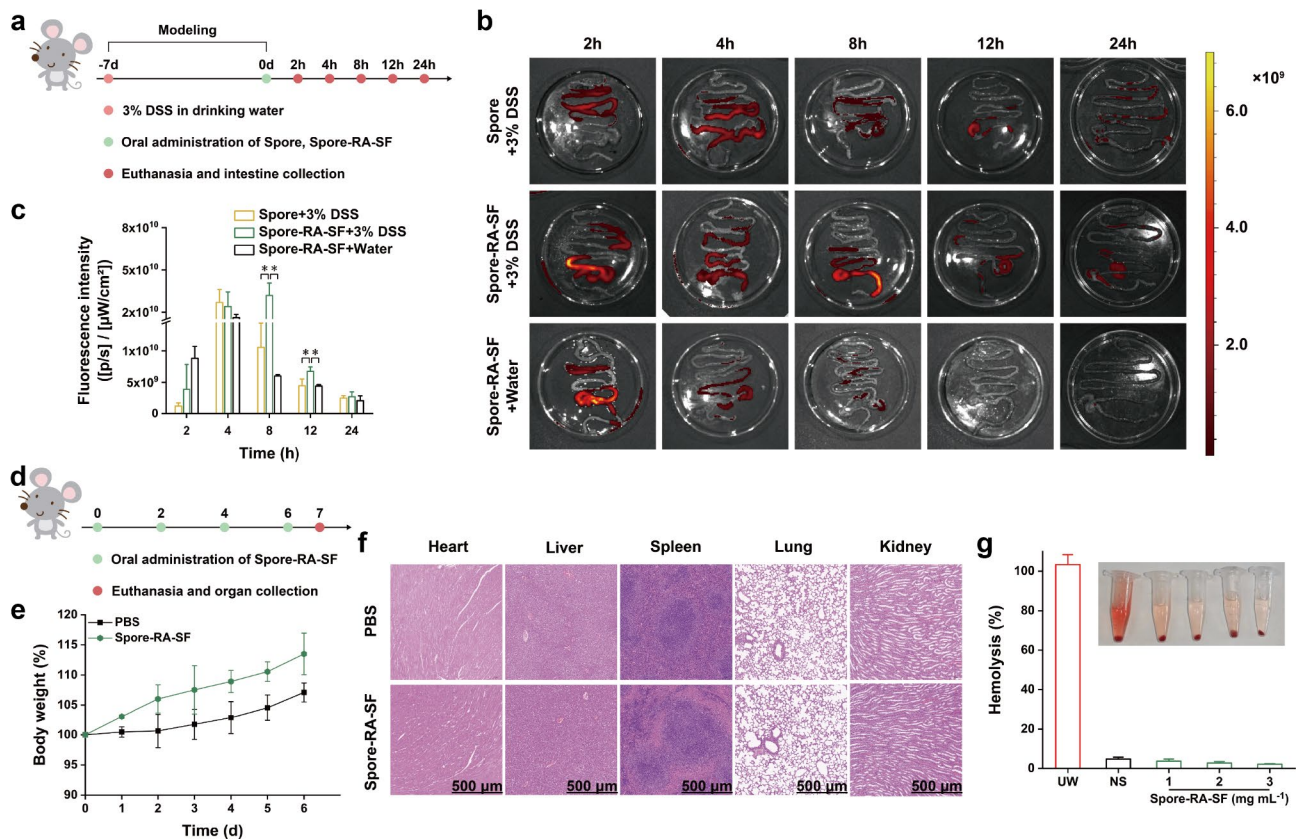


**Fig. 4** In vivo targeting and biosafety of Spore-RA-SF. **(a)** Schematic diagram of in vivo targeting studies in colitis mice. Mice were given water containing 3% DSS for 7 days and then sacrificed at 2, 4, 8, 12, or 24 h after oral administration of FITC-labeled Spore or Spore-RA-SF, and the intestines were collected for IVIS imaging. **(b)** Representative fluorescence images of the healthy and colitis mouse intestines at different time points (2, 4, 8, 12, and 24 h) after oral administration of Spore or Spore-RA-SF. **(c)** Region-of-interest (colon) analysis of fluorescence intensities of the healthy and colitis mouse intestines. **(d)** Schematic diagram of in vivo biosafety assessment. Mice were orally administered Spore-RA-SF on days 0, 2, 4, and 6 and sacrificed on day 7 to collect the major organs. **(e)** Body weight changes of the healthy mice treated with PBS or Spore-RA-SF. **(f)** Representative H&E staining images of major organs of the healthy mice after PBS or Spore-RA-SF treatment. Scale bar: 500  $\mu$ m. **(g)** Representative hemolysis photos and corresponding quantified data of mouse serum treated with ultrapure water, normal saline, and different concentrations of Spore-RA-SF. UW: ultrapure water. NS: normal saline. Data were presented as the mean  $\pm$  standard deviation ( $n=3$  biologically independent samples). Statistical analysis was evaluated with two-tailed Student's *t* tests (\* $P < 0.05$ , \*\* $P < 0.01$ , \*\*\* $P < 0.001$ , \*\*\*\* $P < 0.0001$ )

dilution curve of each group tended to be flat, indicating that the sequencing depths were sufficient for further species analysis (Supplementary Fig. 9). The results showed that oral administration of Spore-RA-SF could significantly grow the species and  $\alpha$ -diversity of gut microbiota in colitis mice (Fig. 6a, b and Supplementary Fig. 10).  $\beta$ -diversity indicates differences in microbiota composition. Principal component analysis (PCA) and principal coordinate analysis (PCoA) showed that DSS treatment prominently damaged the gut microbiota composition of mice, while Spore-RA-SF treatment largely restored it to a normal level (Fig. 6c and Supplementary Fig. 11). Analysis at the phylum level revealed that DSS treatment significantly decreased the relative abundance of Firmicutes and increased the relative abundance of Proteobacteria in the mouse intestines, which is a characteristic of gut microbiota dysbiosis in IBD patients. After different treatments, especially Spore-RA-SF

treatment, the relative abundances of Firmicutes and Proteobacteria were remarkably reversed (Fig. 6d-f). The gut microbiota composition of colitis mice after treatment was further disclosed at the family level, and we discovered that Spore-RA-SF treatment significantly restored Muribaculaceae and Lachnospiraceae that were reduced due to DSS treatment (Fig. 6g, h). These two families are closely related to the production of short-chain fatty acids (SCFAs). The ternary plot analysis at the genus level showed that Spore-RA-SF treatment significantly increased Akkermansia (could ameliorate colitis by regulating CD8<sup>+</sup> cytotoxic T cells) and Lachnospiraceae\_NK4A136\_group (associated with butyrate production) and decreased Escherichia\_Shigella (a toxic pathogen that exacerbates IBD) in the intestine of colitis mice (Fig. 6i-l). To further explain the observed differences in microbiota composition, we conducted a linear discriminant analysis (LDA) effect size (LEfSe) analysis

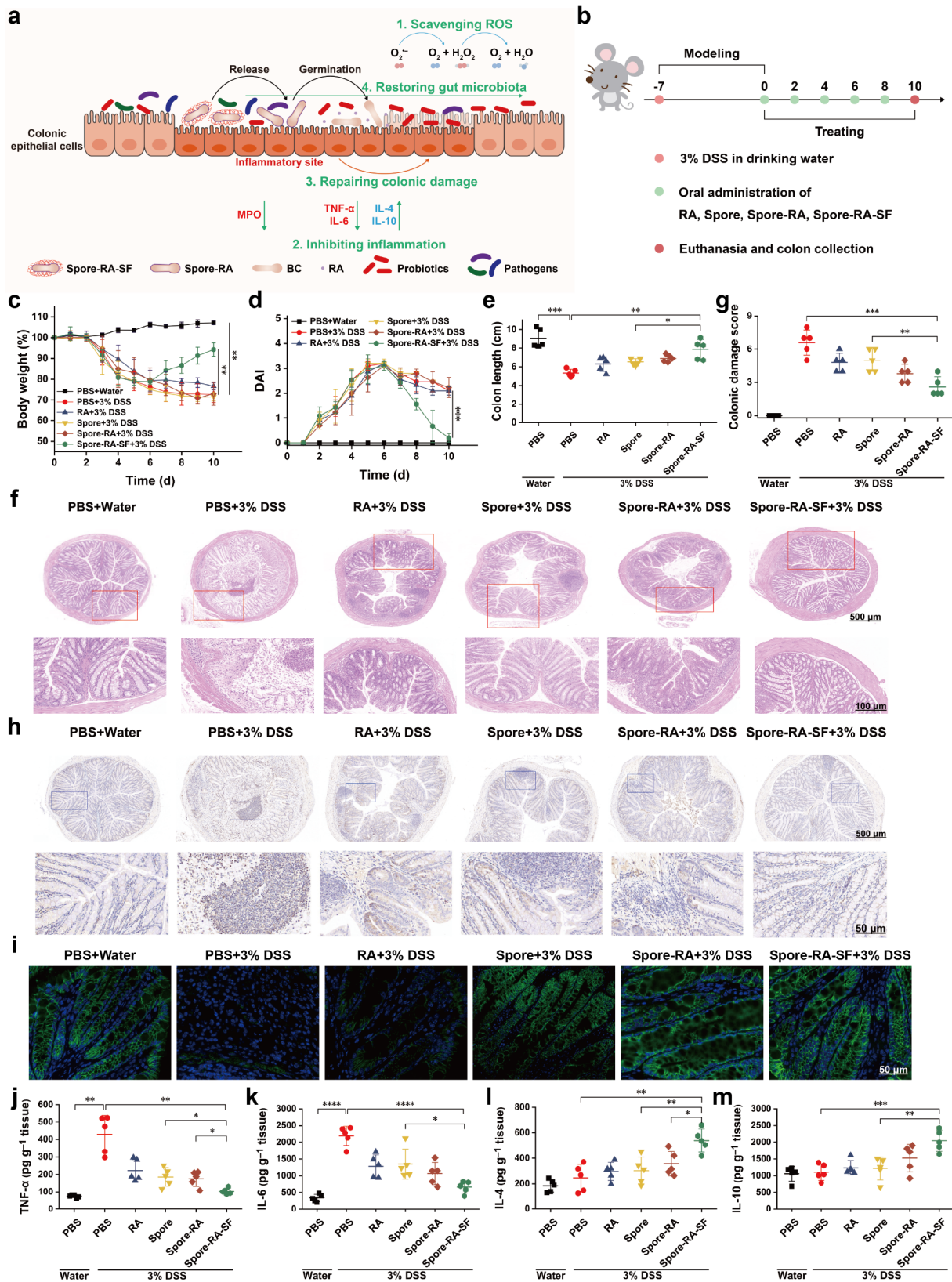


**Fig. 5** (See legend on next page.)

(See figure on previous page.)

**Fig. 5** Therapeutic efficacy of Spore-RA-SF against mouse colitis. **(a)** Schematic diagram of Spore-RA-SF scavenging ROS, inhibiting inflammation, repairing colonic damage, and restoring gut microbiota in the inflamed colon. **(b)** Schematic diagram of the treatment in DSS-induced mouse colitis. Mice were given water containing 3% DSS for 7 days and then given various oral treatment formulas (RA, Spore, Spore-RA, or Spore-RA-SF) on days 0, 2, 4, 6, and 8. Finally, the mice were sacrificed on day 10, and the colons were collected. **(c)** Body weight and **(d)** DAI changes of mice in each group during the treatment. **(e)** Quantified lengths of mouse colons on day 10 after different treatments. **(f)** Representative H&E staining images of mouse colons after different treatments. Scale bar: 500  $\mu\text{m}$  and 100  $\mu\text{m}$ . **(g)** Colonic damage scores of mice after different treatments. **(h)** Immunohistochemical staining images to evaluate the colonic MPO levels in each group. Scale bar: 500  $\mu\text{m}$  and 50  $\mu\text{m}$ . **(i)** Immunofluorescence staining images to evaluate the colonic occludin levels in each group. Blue: DAPI. Green: occludin. Scale bar: 50  $\mu\text{m}$ . **(j-m)** Levels of TNF- $\alpha$ , IL-6, IL-4, and IL-10 in the colon tissues measured by enzyme-linked immunosorbent assay (ELISA) on day 10 after different treatments. Data were presented as the mean  $\pm$  standard deviation ( $n = 5$  biologically independent samples). Statistical analysis was evaluated with two-tailed Student's  $t$  tests (\* $P < 0.05$ , \*\* $P < 0.01$ , \*\*\* $P < 0.001$ , \*\*\*\* $P < 0.0001$ )

(Fig. 6m, n). Consistent with the aforementioned findings, there were significant decreases in the abundance of Muribaculaceae and Lachnospiraceae\_NK4A136\_group in the intestine of colitis mice, while Proteobacteria and Escherichia\_Shigella that are related to IBD were remarkably enriched (LDA ( $\log_{10}$ ) > 4.0). After Spore-RA-SF treatment, these harmful bacteria associated with IBD decreased, while the beneficial Muribaculaceae were significantly enriched compared with other treatment groups. All of the above results confirmed that Spore-RA-SF treatment prominently improved the relative abundance of beneficial bacteria and reduced the relative abundance of harmful bacteria in the intestine of colitis mice, thereby regulating gut microbiota and alleviating intestinal inflammation.

#### Potential signaling pathways for the therapeutic effects of Spore-RA-SF

To further reveal the potential molecular mechanism of Spore-RA-SF in IBD treatment, we performed RNA sequencing of colon tissues in different groups of mice [57]. As shown in PCA, there was a significant difference in gene expression between the Spore-RA-SF and DSS groups, and the gene expression of colitis mice after Spore-RA-SF treatment was similar to that of healthy mice (Fig. 7a). Meanwhile, the gene expression correlation matrix exhibited an analogous analysis result (Fig. 7b). Compared with the untreated DSS group, 602 genes were upregulated and 1094 genes were downregulated prominently after Spore-RA-SF treatment ( $|\log_2(\text{fold change})| \geq 1.0$ ) (Fig. 7c). Differential expressed genes (DEGs) in the heatmap showed that the expression of inflammation-related genes (*Ackr3*, *Ccl9*, *Il1r2*, *Il6st*, *Il34*, *Il1r1*, *Il6ra*, *F2r*, etc.) was downregulated by Spore-RA-SF treatment (Fig. 7d). Through Gene Ontology (GO) and Kyoto Encyclopedia of Genes and Genomes (KEGG) enrichment analysis, we further explored the biological functions and main enrichment pathways of these DEGs. The GO annotation in aspects of biological process (BP), cellular component (CC), and molecular function (MF) indicated that the DEGs between the DSS and Spore-RA-SF groups primarily focused on apoptotic process (GO:0007263), extracellular nucleoid (GO:0044754), and protein kinase activity

(GO:0008239) (Fig. 7e). GO enrichment analysis revealed that these DEGs were mainly associated with extracellular space, extracellular matrix, extracellular region, and inhibin–betaglycan–ActRII complex (Fig. 7f). The extracellular matrix contains various secreted proteins (including cytokines, chemokines, etc.), and its chemical composition and mechanical properties can be altered by inflammation and injury, thereby altering a large number of immune processes; Activin A regulates inflammation through the activin type II receptor (ActRII), while betaglycan binding inhibin mediates functional antagonism of activin signaling [58, 59]. As a result, the downregulation of the aforementioned pathways implied inhibition of overactive inflammatory responses. KEGG enrichment analysis showed that Spore-RA-SF treatment downregulated complement and coagulation cascades, PI3K–Akt signaling pathway, MAPK signaling pathway, and AGE–RAGE signaling pathway, whose activation is associated with inflammatory responses (Fig. 7g). Furthermore, Gene Set Enrichment Analysis (GSEA) demonstrated that “Inflammatory bowel disease”, “PI3K–Akt signaling pathway”, “NF– $\kappa$ B signaling pathway”, “TNF signaling pathway”, “IL-17 signaling pathway”, and “Cytokine–cytokine receptor interaction” were significantly inhibited by Spore-RA-SF treatment (Fig. 7h, i and Supplementary Fig. 12). The downregulated genes of some pathways were shown in the KEGG annotation map (Supplementary Fig. 13–16). Protein–protein interaction network analysis identified the crucial role of the *Mmp9* gene in the DSS-induced colitis occurrence and the Spore-RA-SF-shut colitis (Fig. 7j). Moreover, we validated the changes in relative expression levels of the critical genes (*Mmp9*, *Fgf2*, *Itgb3*, *Cdh2*, *Tgfb3*, and *Thbs1*) by reverse transcription quantitative polymerase chain reaction (RT-qPCR) tests. These genes were remarkably upregulated in the DSS group and downregulated in the Spore-RA-SF group (Fig. 7k–p). Together, Spore-RA-SF may alleviate colitis in mice by downregulating the transcription levels of various pro-inflammatory cytokines and chemokines, and *Mmp9* gene likely has important significance in anti-inflammatory therapy.

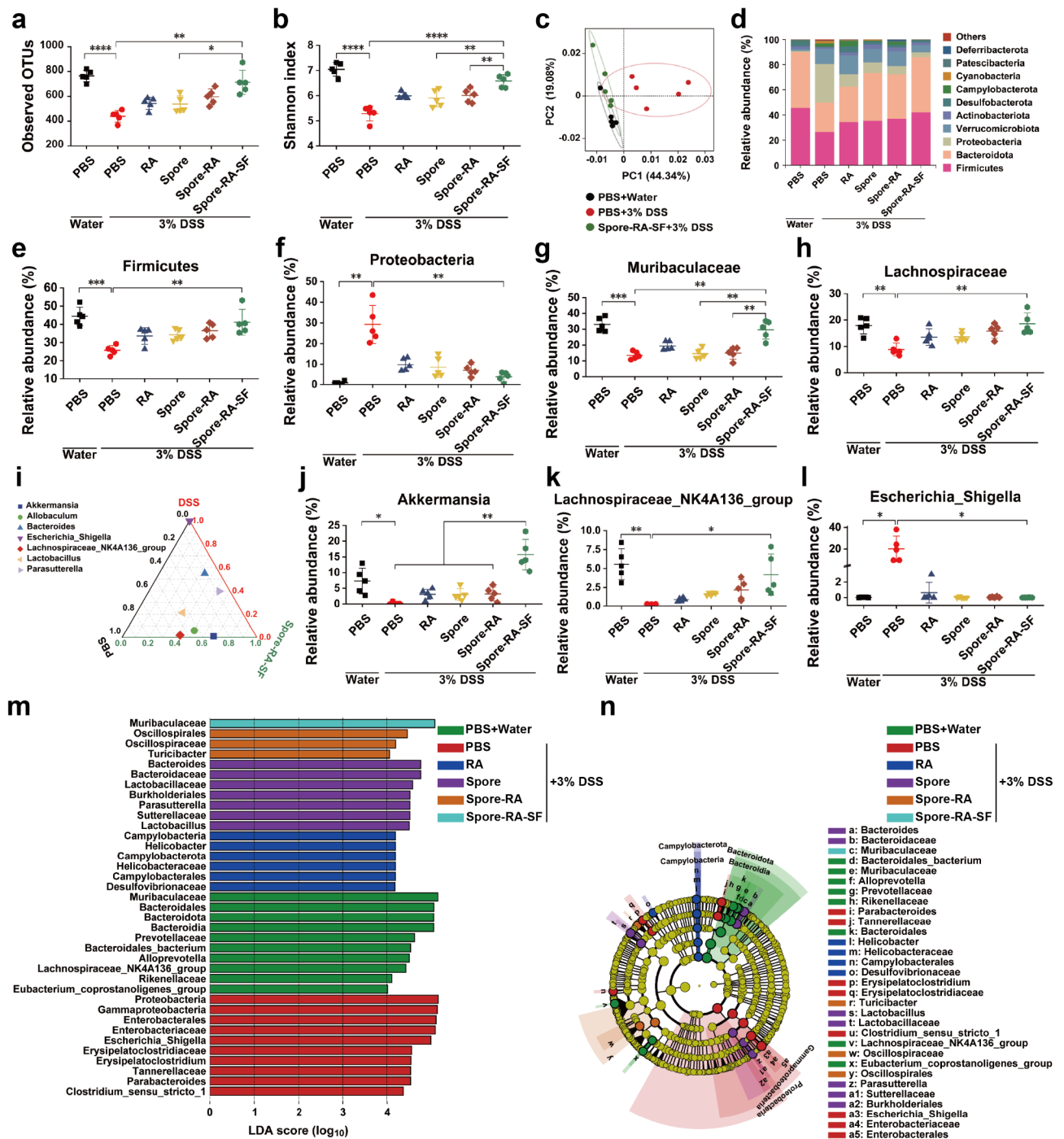


**Fig. 6** Modulation of gut microbiota by Spore-RA-SF. **(a)** Operational taxonomic units (OTUs) of the mouse gut microbiota after different treatments. **(b)** Shannon index ( $\alpha$ -diversity) of gut microbiota in different groups of mice. **(c)** PCA ( $\beta$ -diversity) of gut microbiota in different groups of mice. **(d)** Phylum-level taxonomy presented as a percentage of the total sequences in each group. **(e), (f)** Relative abundance of Firmicutes and Proteobacteria (phylum-level) after different treatments. **(g), (h)** Relative abundance of Muribaculaceae and Lachnospiraceae (family-level) after different treatments. **(i)** Ternary plot of mouse gut microbiota at genus-level taxonomy. **(j-l)** Relative abundance of Akkermansia, Lachnospiraceae\_NK4A136\_group, and Escherichia\_Shigella (genus-level) after different treatments. **(m)** Taxa listed according to their LDA values determined from comparisons between each group using the LEfSe method. **(n)** Cladogram based on LEfSe analysis exhibiting the community composition of the mouse gut microbiota in different groups. Data were presented as the mean  $\pm$  standard deviation ( $n=5$  biologically independent samples). Statistical analysis was evaluated with two-tailed Student's  $t$  tests ( $*P < 0.05$ ,  $**P < 0.01$ ,  $***P < 0.001$ ,  $****P < 0.0001$ )

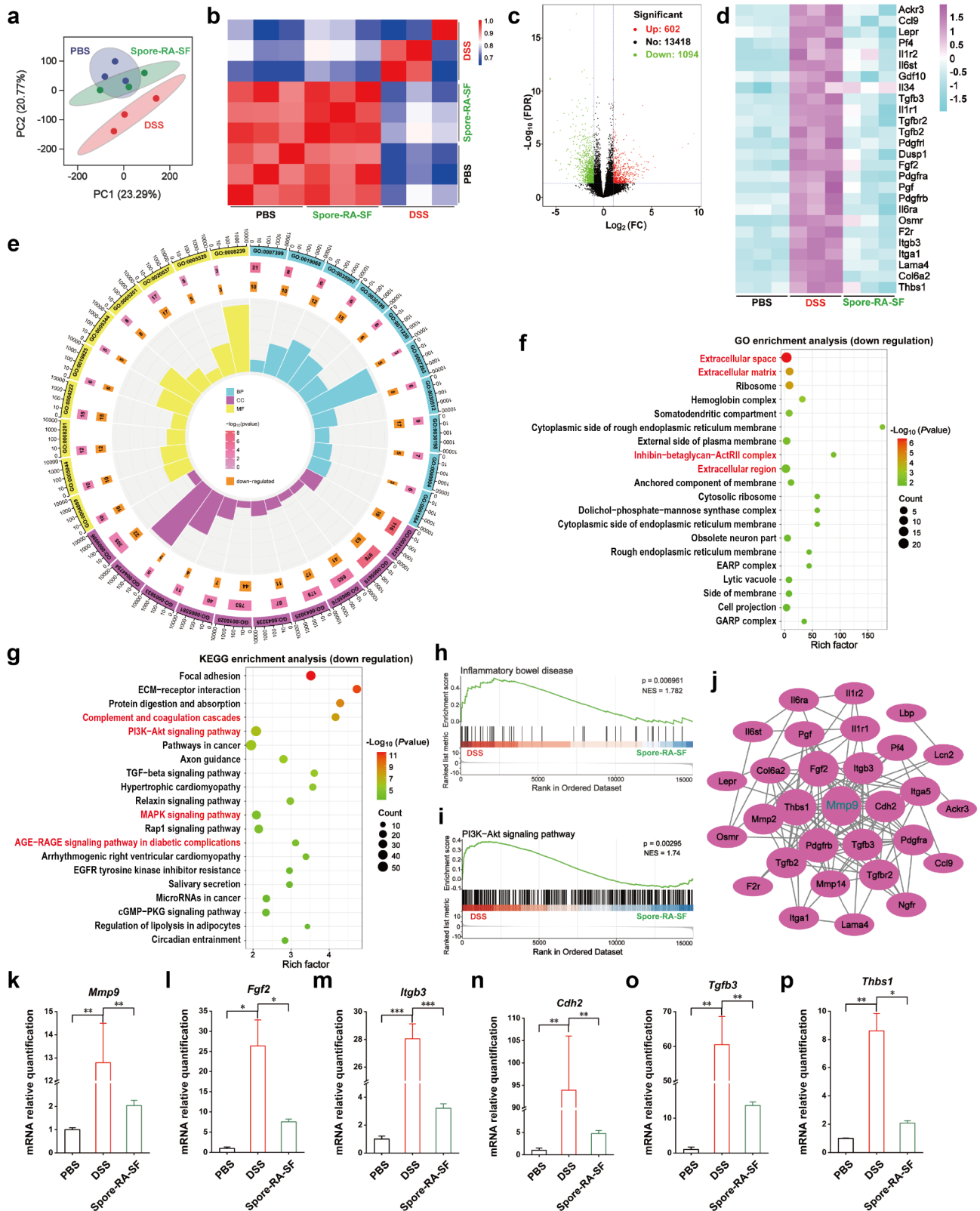


Fig. 7 (See legend on next page.)

(See figure on previous page.)

**Fig. 7** Potential signaling pathways for the therapeutic effects of Spore-RA-SF. **(a)** PCA revealed gene expression differences in the colons of different groups of mice. **(b)** Correlation matrix map revealed gene expression differences in the colons of different groups of mice. **(c)** Volcano plot of DEGs. Red dots indicated upregulated genes, and green dots indicated downregulated genes. **(d)** Heatmap showed significantly downregulated genes in the colon of colitis mice after Spore-RA-SF treatment. **(e)** GO enrichment analysis between DSS and Spore-RA-SF group mice based on the BP, CC, and MF annotation. **(f), (g)** GO and KEGG enrichment analyses revealed differential metabolic pathways in the mouse colon. **(h), (i)** GSEA plots indicated the suppressed signaling pathways (Inflammatory bowel disease and PI3K–Akt signaling pathway) in the colon of colitis mice after Spore-RA-SF treatment. **(j)** Protein–protein interaction network revealed that Spore-RA-SF treatment reversed the expression of potential target genes in the inflamed colon. **(k–p)** mRNA relative levels of *Mmp9*, *Fgf2*, *Itgb3*, *Cdh2*, *Tgfb3*, and *Thbs1* genes in colon tissues of mice from different treatment groups by RT-qPCR tests. Data were presented as the mean  $\pm$  standard deviation ( $n=3$  biologically independent samples). Statistical analysis was evaluated with two-tailed Student's *t* tests (\* $P<0.05$ , \*\* $P<0.01$ , \*\*\* $P<0.001$ , \*\*\*\* $P<0.0001$ )

## Conclusion

In this work, we developed probiotic BC spores encapsulated by the natural anti-inflammatory and antioxidant molecule RA and the biocompatible molecule SF, achieving the effective treatment of DSS-induced colitis in mice. Our probiotic composite materials were discovered to inhibit the growth of *E. coli* DH5 $\alpha$  through the consumption of dissolved oxygen in the culture medium and scavenge a diverse range of ROS/RNS efficiently, such as ABTS<sup>+</sup>, DPPH $\cdot$ , PTIO $\cdot$ , O<sub>2</sub><sup>-</sup>, and H<sub>2</sub>O<sub>2</sub>. Excitingly, the combined use of SF protected the ROS/RNS scavenging activities of RA in the simulated gastrointestinal environment and enhanced the targeting ability of probiotics towards the inflamed intestine, thus significantly improving their oral bioavailability. In addition, the probiotic composite materials had no adverse effects on healthy mice. In the treatment of mouse colitis, they prominently alleviated a series of colitis symptoms, such as weight loss, increased DAI, and colon shortening and lesions. Meanwhile, MPO activity and inflammatory factor storms (increased levels of TNF- $\alpha$  and IL-6) in colon tissue were remarkably inhibited. The 16 S rRNA sequencing analysis of colonic contents revealed that Spore-RA-SF treatment significantly restored the disturbed gut microbiota of colitis mice, including the rising levels of Firmicutes, Muribaculaceae, Lachnospiraceae, Akkermansia, and Lachnospiraceae\_NK4A136\_group, as well as the reduced levels of Proteobacteria and *Escherichia Shigella*. Furthermore, the mRNA sequencing analysis of colon tissue showed that the probiotic composite materials downregulated inflammation-related signaling pathways such as PI3K–Akt signaling pathway, MAPK signaling pathway, and AGE–RAGE signaling pathway. Concurrently, *Mmp9* gene likely has important significance in anti-inflammatory therapy. Overall, our strategy of modifying probiotics with therapeutic nano-coating may open up novel avenues for future microbial therapy for IBD. However, the lack of long-term fluorescent labeling methods for BC made it uncertain whether the nano-coating could effectively prolong its colonization in inflamed intestines. Furthermore, this study lacked exploration of the long-term biosafety and therapeutic molecular mechanisms of the probiotic composite

materials; thus, it remained unclear whether it had any chronic effects on animals.

## Methods

### Materials

*Bacillus coagulans* (BC) was purchased from BeNa Culture Collection. Rosmarinic acid (RA) was obtained from Shanghai Macklin Biochemical Technology Co., Ltd. Silk fibroin (SF) was extracted from tussah silkworms. 1-(3-dimethylaminopropyl)-3-ethylcarbodiimide (EDC) and *N*-hydroxysuccinimide (NHS) were purchased from Shanghai Macklin Biochemical Technology Co., Ltd. Enterobacteriaceae selective MacConkey agar plates were obtained from Qingdao Rishui Bio-Technologies Co., Ltd. 2,2'-azino-bis(3-ethyl-benzothiazoline-6-sulfonic acid) diammonium salt (ABTS), 1,1-diphenyl-2-picrylhydrazyl (DPPH), and 2-phenyl-4,4,5,5-tetramethylimidazole-3-oxide-1-oxyl (PTIO) were purchased from Shanghai Titan Scientific Co., Ltd. Pepsin and trypsin were obtained from Shanghai Macklin Biochemical Technology Co., Ltd. Dextran sulfate sodium (DSS, M.W. 36,000–50,000) was purchased from Regent Science Industry Limited. Institute of Cancer Research (ICR) female mice were obtained from Hunan SJA Laboratory Animal Co., Ltd. Fluorescein isothiocyanate (FITC) was purchased from Shanghai Macklin Biochemical Technology Co., Ltd. Enzyme-linked immunosorbent assay (ELISA) kits were obtained from MultiSciences Biotech Co., Ltd. FreeZol Reagent R711 kit was purchased from Nanjing Vazyme Biotech Co., Ltd. *Evo M-MLV* RT Mix Kit with gDNA Clean for qPCR Ver.2 and SYBR Green Premix *Pro Taq* HS qPCR Kit were obtained from Accurate Biotechnology (Hunan) Co., Ltd.

### Spore preparation

Spores were prepared using MRS medium supplemented with 0.05% MnSO<sub>4</sub>·H<sub>2</sub>O as sporulation medium. 100 mL of sporulation medium was inoculated with 200  $\mu$ L of activated BC and incubated with shaking at 150 rpm for 48 h at 37  $^{\circ}$ C. After 48 h, the medium was heated in an 80  $^{\circ}$ C water bath for 30 min to ensure the killing of vegetative cells. The spores were collected by centrifugation at 10,000 rpm for 30 min at 4  $^{\circ}$ C and washed three times

with 1 M KCl/0.5 M NaCl solution, then resuspended in ultrapure water and stored at -20 °C.

#### Preparation of Spore-RA and Spore-RA-SF

RA was dissolved in ultrapure water, mixed with EDC and NHS at a ratio of 3:3:1, and incubated at 150 rpm for 1 h at 37 °C to activate carboxyl groups. Then, the purified spores were added to the mixed solution and incubated with shaking at 150 rpm for 24 h at 37 °C. After 24 h of reaction, the mixed solution was centrifuged at 4000 rpm for 5 min at 4 °C to collect Spore-RA, then Spore-RA was washed three times with phosphate buffer (pH 6.0) containing 0.01 M Na<sup>+</sup>. To prepare Spore-RA-SF, 0.1% (w/v) SF was added to the resuspended Spore-RA under shaking at 35 rpm for 10 min. The mixed solution was centrifuged at 4000 rpm for 3 min at 4 °C, and cells were washed once with ultrapure water. Then, the cells were resuspended in phosphate buffer (pH 5.5) containing 0.1 M K<sup>+</sup> and shaken vigorously at 1000 rpm for 10 min. After centrifuging the mixed solution and washing cells again, Spore-RA-SF was collected by centrifugation at 10,000 rpm for 5 min at 4 °C. After repeating the above steps four times, the Spore-RA-SF with multi-layer coating was obtained. Spore, Spore-RA, and Spore-RA-SF were characterized using scanning electron microscopy (SEM), atomic force microscopy (AFM), nanoparticle size, zeta potential, Fourier transform infrared (FT-IR) spectroscopy, nuclear magnetic resonance (NMR) spectroscopy, circular dichroism (CD), and fluorescence microscopy. The activities of Spore, Spore-RA, and Spore-RA-SF were determined by the plate-counting method.

#### Measurement of growth curves

100 mL of MRS medium was inoculated with equal amounts of Spore, Spore-RA, or Spore-RA-SF. Beginning at 0 h, 0.1 mL of the medium was taken and diluted 10 times every 2 h, and its absorbance at 600 nm was measured.

#### Bacteriostatic test

100 mL of LB medium was inoculated with equal amounts of Spore, Spore-RA, or Spore-RA-SF and incubated statically for 10 h at 37 °C, and then 200 µL or 2 mL of *Escherichia coli* (*E. coli*) DH5α was inoculated into the medium. After incubation for 12 h at 37 °C, the medium was diluted 100,000 times and spread on Enterobacteriaceae selective MacConkey agar plates, which were then incubated for 12 h at 37 °C. The colonies on the plates were observed and counted to evaluate the inhibitory effect of spores on *E. coli* DH5α.

#### Dissolved oxygen assay

Beginning at 0 h, the medium of Spore or Spore-RA-SF was transferred to dissolved oxygen bottles every 2 h. 1 mL of 2.15 M MnSO<sub>4</sub> solution and 2 mL of 0.90 M alkaline KI solution were added below the liquid level successively using pipettes, and then the bottles were inverted and mixed 15 times. When the brown flocculent sediment in the bottles dropped to half, the bottles were inverted and mixed several times again. Before analysis, the bottle caps were opened gently, and 2 mL of sulfuric acid (pH 1.84) was added below the liquid level using pipettes. After all the sediment was dissolved, the bottles were placed in the dark for 5 min. 100 mL of the above solution was transferred into 250 mL conical flasks and then titrated with 0.0129 M Na<sub>2</sub>S<sub>2</sub>O<sub>3</sub> standard solution until it turned slightly yellow. Finally, 1 mL of 1% starch solution was added to the solution, which was then titrated continually with Na<sub>2</sub>S<sub>2</sub>O<sub>3</sub> solution until the blue just faded away. Dissolved O<sub>2</sub> (mg L<sup>-1</sup>) = 1.032 × V (V represents the volume (mL) of Na<sub>2</sub>S<sub>2</sub>O<sub>3</sub> standard solution consumed by titration).

#### ROS/RNS scavenging abilities

**ABTS assay:** Firstly, 7 mM ABTS solution was mixed with 2.45 mM K<sub>2</sub>S<sub>2</sub>O<sub>8</sub> in the dark for 12–16 h to obtain ABTS<sup>•+</sup> solution, which was then diluted until the absorbance at 734 nm reached about 0.7 ± 0.2. Then, 100 µL of different materials with the same concentration were mixed with 3.9 mL of ABTS<sup>•+</sup> working solution. After 20 min of incubation at room temperature, the absorbance at 734 nm of the reaction solution was determined. ABTS<sup>•+</sup> scavenging capacity was assessed through Equation:

ABTS<sup>•+</sup> scavenging ratio (%) =  $(A_b - A_s) / A_b \times 100\%$  ( $A_b$  and  $A_s$  represent the absorbance at 734 nm of the original ABTS<sup>•+</sup> solution and reacted ABTS<sup>•+</sup> solution, respectively.)

**DPPH assay:** Firstly, 2 mg of DPPH was dissolved in 24 mL of absolute ethanol and sonicated for 5 min for sufficient dissolution. Then, 100 µL of different materials with the same concentration were mixed with 3.9 mL of DPPH<sup>•</sup> solution. After 30 min of incubation in a 37 °C water bath, the absorbance at 519 nm of the reaction solution was determined. DPPH<sup>•</sup> scavenging capacity was assessed through Equation:

DPPH<sup>•</sup> scavenging ratio (%) =  $(A_b - A_s) / A_b \times 100\%$  ( $A_b$  and  $A_s$  represent the absorbance at 519 nm of the original DPPH<sup>•</sup> solution and reacted DPPH<sup>•</sup> solution, respectively.)

**PTIO assay:** Firstly, 3 mg of PTIO was dissolved in 20 mL of ultrapure water and sonicated for 5 min for sufficient dissolution. Then, 100 µL of different materials with the same concentration were mixed with 3.9 mL of PTIO<sup>•</sup> solution. After 2 h of incubation in a 37 °C water

bath, the absorbance at 557 nm of the reaction solution was determined. PTIO• scavenging capacity was assessed through Equation:

PTIO• scavenging ratio (%) =  $(A_b - A_s) / A_b \times 100\%$  ( $A_b$  and  $A_s$  represent the absorbance at 557 nm of the original PTIO• solution and reacted PTIO• solution, respectively.)

$O_2^{\cdot-}$  assay: Firstly, 20  $\mu$ M riboflavin, 12.5 mM methionine, 75  $\mu$ M nitroblue tetrazolium (NBT), and different materials with the same concentration were mixed in PBS (pH 7.4). Then, the mixed solution was constantly illuminated for 15 min at room temperature. After the reaction, the mixed solution was centrifuged at 4000 rpm for 3 min, and the absorbance at 560 nm of the supernatant was determined.  $O_2^{\cdot-}$  scavenging capacity was assessed through Equation:

$O_2^{\cdot-}$  scavenging ratio (%) =  $(A_0 - A_n) / (A_p - A_n) \times 100\%$  ( $A_0$ ,  $A_n$ , and  $A_p$  represent the absorbance at 560 nm of the sample, negative control, and positive control, respectively.)

$H_2O_2$  assay: Firstly, 0.1 g of  $(NH_4)_6Mo_7O_{24} \cdot 4H_2O$  was dissolved in 250 mL of 0.5 M  $H_2SO_4$  to obtain molybdate chromogenic agent. Then, 100 mM  $H_2O_2$  and different materials with the same concentration were mixed in PBS. After 30 min of incubation in a 37 °C water bath, the reaction solution was mixed with an equal volume of molybdate chromogenic agent. Then, the absorbance at 330 nm of the mixed solution was determined.  $H_2O_2$  scavenging capacity was assessed through Equation:

$H_2O_2$  scavenging ratio (%) =  $(A_0 - A_n) / (A_p - A_n) \times 100\%$  ( $A_0$ ,  $A_n$ , and  $A_p$  represent the absorbance at 330 nm of the sample, negative control, and positive control, respectively.)

#### Survival of Spore, Spore-RA, and Spore-RA-SF after simulated gastrointestinal fluid treatment

Preparation of simulated gastric fluid (SGF): 3.2 g pepsin and 2.0 g NaCl were dissolved in 500 mL ultrapure water, and 7 mL concentrated hydrochloric acid was mixed in the solution, which was then adjusted the pH to 2.0 with dilute hydrochloric acid. The mixed solution was supplemented with ultrapure water to a total volume of 1 L, and SGF (pH 2.0) was obtained by filtering the mixed solution with a 0.22  $\mu$ m filter membrane.

Preparation of simulated intestinal fluid (SIF): 6.8 g  $KH_2PO_4$  was dissolved in 450 mL ultrapure water, and 77 mL 0.2 M NaOH and 10 g trypsin were mixed in the solution, which was then adjusted the pH to 6.8 with dilute hydrochloric acid. The mixed solution was supplemented with ultrapure water to a total volume of 1 L, and SIF (pH 6.8) was obtained by filtering the mixed solution with a 0.22  $\mu$ m filter membrane.

Preparation of simulated colonic fluid (SCF): 5.59 g dipotassium hydrogen phosphate and 0.41 g potassium

dihydrogen phosphate were dissolved in 1 L ultrapure water, which was then adjusted the pH to 7.8. SCF (pH 7.8) was obtained by filtering the mixed solution with a 0.22  $\mu$ m filter membrane.

Equal amounts of Spore, Spore-RA, or Spore-RA-SF were incubated in SGF, SIF, or SCF for 1 h at 37 °C. The incubated solution was diluted 1,000,000 times and spread on MRS agar plates, which were then incubated for 24 h at 37 °C. The colonies on the plates were observed and counted to evaluate the survival of Spore, Spore-RA, and Spore-RA-SF after simulated gastrointestinal fluid treatment.

#### ROS/RNS scavenging capacities in simulated gastrointestinal environment

Equal amounts of Spore-RA or Spore-RA-SF were incubated in SGF, SIF, or SCF for 1 h at 37 °C. After incubation, ROS/RNS scavenging capacities were determined by the above methods.

#### In vivo targeting test

Forty-five mice were divided into three groups (fifteen mice per group), and the drinking water of two groups was supplemented with 3% DSS for 7 d to induce colitis after adapting to the environment for one week. Next, mice in the normal group were orally administered FITC-labeled Spore-RA-SF ( $5 \times 10^8$  CFU per mouse), and mice in the two groups with colitis were orally administered FITC-labeled Spore or Spore-RA-SF ( $5 \times 10^8$  CFU per mouse), respectively. At 2, 4, 8, 12, or 24 h after oral administration, the mice were sacrificed (three mice per group at each time point), and the intestines were collected for in vivo imaging system (IVIS) imaging.

#### Biosafety assessment

Six mice were divided into two groups (three mice per group) and orally administered the same volume of PBS or Spore-RA-SF ( $5 \times 10^8$  CFU per mouse) on days 0, 2, 4, and 6. The weight of the mice was observed every day. The mice were sacrificed on day 7, and their blood samples were collected from the orbital venous sinus for the erythrocyte hemolysis test. The major organs (heart, liver, spleen, lung, and kidney) were also collected for histopathological evaluation by hematoxylin and eosin (H&E) staining.

Erythrocyte hemolysis test: Mouse orbital venous sinus blood samples collected with anticoagulant tubes were centrifuged at 3000 rpm for 5 min at 4 °C. After removing the supernatant, the precipitate was washed three times with normal saline. The obtained blood cell solution was mixed with normal saline at a volume ratio of 4:5, and then 0.2 mL of the suspension was mixed with 5 mL of ultrapure water, normal saline, or different concentrations of Spore-RA-SF for 30 min at 37 °C. After

additional incubation for 1 h at 37 °C, the solution was centrifuged at 3000 rpm for 5 min, and the absorbance at 545 nm of the supernatant was measured.

**Histopathological evaluation:** The collected tissues were fixed in 4% paraformaldehyde for 24 h, and then rinsed with running water for 1 h to remove excess fixative. After alcohol dehydration and xylene treatment, the tissues were embedded in paraffin and sectioned. The sections were dewaxed and H&E stained after being fixed to glass slides. Finally, the sections were observed with optical microscopy for histopathological evaluation.

#### **Therapeutic efficacy against mouse colitis**

Thirty mice were divided into six groups (five mice per group), and the drinking water of five groups was supplemented with 3% DSS for 7 d to induce colitis after adapting to the environment for one week. Next, mice in the four groups with colitis were orally administered RA (5 mg kg<sup>-1</sup>), Spore, Spore-RA, or Spore-RA-SF (5 × 10<sup>8</sup> CFU per mouse) on days 0, 2, 4, 6, and 8, respectively. Mice in the other group with colitis and in the normal group were orally administered equal amounts of PBS. During the treatment, the weight of the mice was recorded every day. On day 10, the mice were sacrificed, their colons were collected and photographed, and the colon length was recorded.

#### **Disease activity assay**

During the treatment, the body weight, stool consistency, and hematochezia of mice with different treatments were recorded every day. Disease activity index (DAI) was calculated according to the scoring schemes of DAI parameters in Supplementary Table 1 (the final score was the average of the scores of various parameters).

#### **Colonic damage assessment**

The distal colons of mice were subjected to H&E staining and observed by optical microscopy. The colonic damage score was assessed in a blinded fashion to avoid observer bias, according to the histological grading schemes in Supplementary Table 2 (the final score was the sum of the scores of colonic epithelial damage and inflammatory cell infiltration).

#### **Myeloperoxidase (MPO) activity detection**

The MPO activity in the colon tissues of mice was detected by an immunohistochemical test and observed by optical microscopy.

#### **Colon tissue cytokine detection**

Colon tissues were soaked in PBS at a w/v ratio of 1:10 and then homogenized. The concentrations of tumor necrosis factor- $\alpha$  (TNF- $\alpha$ ), interleukin-6 (IL-6), IL-4, and IL-10 in colon tissues were determined by ELISA kits.

#### **Gut microbiota analysis**

Fresh mouse colon contents were snap frozen in liquid nitrogen and sent to Biomarker Technologies Co., Ltd. for 16 S ribosomal RNA (16 S rRNA) sequencing. The reads of each sample were spliced using FLASH v1.2.11, and the raw Tags sequence data with a minimum overlap length of 10 bp and a maximum allowable mismatch ratio of 0.2 in the overlap area were obtained. After filtering Tags whose length was less than 75% of the tag length after quality control using Trimmomatic v0.33 and obtaining high-quality Clean Tags, chimeras in Clean Tags were removed by UCHIME v8.1 to obtain high-quality tag sequences. Next, sequences were clustered using USEARCH (v10.0) at a level of 97% similarity to filter OTUs at a threshold of 0.005% of all the sequence numbers. Sequencing results were analyzed on the BMK-Cloud data analysis platform.

#### **Transcriptomic analysis**

Total RNA in the colon tissues of mice was extracted by standard kits, and the concentration and integrity of the RNA were detected using Nanodrop 2000 and Agilent 2100. The library construction and purification of the extracted total RNA were conducted using Hieff NGS Ultima Dual-mode mRNA Library Prep Kit for Illumina (Yeasen Biotechnology (Shanghai) Co., Ltd.) and Hieff NGS DNA selection Beads (Yeasen Biotechnology (Shanghai) Co., Ltd.). The mRNA sequencing was performed at Biomarker Technologies Co., Ltd. using the Illumina NovaSeq 6000 platform.

#### **Reverse transcription quantitative polymerase chain reaction (RT-qPCR) tests**

Total RNA in the colon tissues of mice was extracted by standard kits and quantified. 1  $\mu$ g RNA from each sample was taken for gDNA removal and reverse transcription. Finally, the cDNA was subjected to qPCR (primers listed in Supplementary Table 3) by the SYBR Green method.

#### **Statistical analysis**

All experimental results were presented as the mean  $\pm$  standard deviation. When two groups were compared, two-tailed Student's *t* tests were performed. Statistical significance was expressed as \**P* < 0.05, \*\**P* < 0.01, \*\*\**P* < 0.001, \*\*\*\**P* < 0.0001.

#### **Supplementary Information**

The online version contains supplementary material available at <https://doi.org/10.1186/s12951-025-03240-1>.

Supplementary Material 1

#### **Acknowledgements**

Not applicable.

### Author contributions

Conceptualization: Y.H., L.W., and G.F. Investigation: Y.H., H.C., H.L., L.W., and G.F. Methodology: Y.H., H.C., H.L., and L.W. Validation: H.C., H.L., L.W., and Z.D. Visualization: Y.H., H.C., H.L., Z.D., and Y.F. Writing – original draft: Y.H., H.C., and G.F. Data curation: G.F., A.L., and J.F. Project administration: J.F. Supervision: J.F. Funding acquisition: G.F., Y.F., and J.F. All authors reviewed the manuscript.

### Funding

This work was supported by the Science and Technology Innovation Program of Hunan Province (2023RC3148), the Opening Foundation of the State Key Laboratory of Chemo/Biosensing and Chemometrics, Hunan University (20230754), National Natural Science Foundation of China (22004035, 31672457), the Double first-class construction project of Hunan Agricultural University (CX20190497), National Key Research and Development Program (2021YFD1300205-2), Hunan Poultry Industry Technology System (HARS-06), Postgraduate scientific research innovation project of Hunan Province (CX20230684).

### Data availability

The data related to this work are available from the corresponding authors upon reasonable request.

### Declarations

#### Ethics approval and consent to participate

All Institutional and National Guidelines for the care and use of animals were followed.

#### Consent for publication

The authors confirm that its publication has been approved by all co-authors.

#### Competing interests

The authors declare no competing interests.

#### Author details

<sup>1</sup>College of Bioscience and Biotechnology, Hunan Agricultural University, Changsha 410128, China

<sup>2</sup>Feed Research Institute/Grain Quality & Nutrition Institute, Key Laboratory of Grain and Oil Biotechnology of National Food and Strategic Reserves Administration, Academy of National Food and Strategic Reserves Administration, Beijing 100037, China

Received: 2 November 2024 / Accepted: 18 February 2025

Published online: 08 March 2025

### References

- Nadeem MS, Kumar V, Al-Abbasi FA, Kamal MA, Anwar F. Risk of colorectal cancer in inflammatory bowel diseases. *Semin Cancer Biol.* 2020;64:51–60.
- Shah SC, Itzkowitz SH. Colorectal Cancer in inflammatory bowel disease: mechanisms and management. *Gastroenterology.* 2022;162:715–e7303.
- Eftychi C, et al. Temporally distinct functions of the cytokines IL-12 and IL-23 drive chronic Colon inflammation in response to intestinal barrier impairment. *Immunity.* 2019;51:367–e3804.
- Schirmer M, Garner A, Vlamakis H, Xavier RJ. Microbial genes and pathways in inflammatory bowel disease. *Nat Rev Microbiol.* 2019;17:497–511.
- Cao F, et al. Artificial-enzymes-armed *Bifidobacterium longum* probiotics for alleviating intestinal inflammation and microbiota dysbiosis. *Nat Nanotechnol.* 2023;18:617–27.
- Campieri M, et al. 5-Aminosalicylic acid for the treatment of inflammatory bowel diseases. *Gastroenterology.* 1985;89:701–3.
- Faubion WA, Loftus EV, Harmsen WS, Zinsmeister AR, Sandborn WJ. The natural history of corticosteroid therapy for inflammatory bowel disease: A Population-Based study. *Gastroenterology.* 2001;121:255–60.
- Ben-Horin S, et al. Combination Immunomodulator and antibiotic treatment in patients with inflammatory bowel disease and *Clostridium difficile* infection. *Clin Gastroenterol Hepatol.* 2009;7:981–7.
- Sun M, et al. Emerging nanomedicine and prodrug delivery strategies for the treatment of inflammatory bowel disease. *Chin Chem Lett.* 2022;33:4449–60.
- Li S, Zhang F, Zhang Q. Pathological features-based targeted delivery strategies in IBD therapy: A mini review. *Biomed Pharmacother.* 2022;151:113079.
- Liu J, et al. Mucoadhesive probiotic backpacks with ROS nanoscavengers enhance the bacteriotherapy for inflammatory bowel diseases. *Sci Adv.* 2022;8:eabp8798.
- Jonkers D, Stockbrügger R. Probiotics and inflammatory bowel disease. *J R Soc Med.* 2003;96:167–71.
- Shanahan F. Probiotics in inflammatory bowel disease—therapeutic rationale and role. *Adv Drug Deliv Rev.* 2004;56:809–18.
- Hou Q, et al. *Lactobacillus* accelerates ISCs regeneration to protect the integrity of intestinal mucosa through activation of STAT3 signaling pathway induced by LPLs secretion of IL-22. *Cell Death Differ.* 2018;25:1657–70.
- Wu H, et al. *Lactobacillus reuteri* maintains intestinal epithelial regeneration and repairs damaged intestinal mucosa. *Gut Microbes.* 2020;11:997–1014.
- Zhang C, et al. Bacteria-Induced colloidal encapsulation for probiotic oral delivery. *ACS Nano.* 2023;17:6886–98.
- Xie A, et al. Modified Prebiotic-Based shield armed probiotics with enhanced resistance of Gastrointestinal stresses and prolonged intestinal retention for synergistic alleviation of colitis. *ACS Nano.* 2023;17:14775–91.
- Zhu L, et al. Responsively degradable Nanoarmor-Assisted super resistance and stable colonization of probiotics for enhanced Inflammation-Targeted delivery. *Adv Mater.* 2024;19:e2308728.
- Cook MT, Tzortzis G, Charalampopoulos D, Khutoryanskiy VV. Microencapsulation of probiotics for Gastrointestinal delivery. *J Control Release.* 2021;162:56–67.
- Centurion F, et al. Nanoencapsulation for probiotic delivery. *ACS Nano.* 2021;15:18653–60.
- Li C, Wang Z, Xiao H, Wu F. Intestinal delivery of probiotics: materials, strategies, and applications. *Adv Mater.* 2024;21:e2310174.
- Huang Q, et al. Stimulation-responsive mucoadhesive probiotics for inflammatory bowel disease treatment by scavenging reactive oxygen species and regulating gut microbiota. *Biomaterials.* 2023;301:122274.
- Zhou J, et al. Programmable probiotics modulate inflammation and gut microbiota for inflammatory bowel disease treatment after effective oral delivery. *Nat Commun.* 2022;13:3432.
- Li M, et al. Engineered probiotics with sustained release of interleukin-2 for the treatment of inflammatory bowel disease after oral delivery. *Biomaterials.* 2024;309:122584.
- Huang Y, et al. From probiotic chassis to modification strategies, control and improvement of genetically engineered probiotics for inflammatory bowel disease. *Microbiol Res.* 2024;289:127928.
- Wang Y, et al. *Bacillus coagulans* TL3 Inhibits LPS-Induced Caecum Damage in Rat by Regulating the TLR4/MyD88/NF- $\kappa$ B and Nrf2 Signal Pathways and Modulating Intestinal Microflora. *Oxid. Med. Cell. Longev.* 2022, 5463290 (2022).
- Li L, et al. Different effects of *Bacillus coagulans* vegetative cells and spore isolates on constipation-induced gut microbiota dysbiosis in mice. *Food Funct.* 2022;13:9645–57.
- Yang J, et al. Calcium tungstate microgel enhances the delivery and colonization of probiotics during colitis via intestinal ecological niche occupancy. *ACS Cent Sci.* 2023;9:1327–41.
- Zheng D, et al. Prebiotics-Encapsulated probiotic spores regulate gut microbiota and suppress Colon cancer. *Adv Mater.* 2020;32:e2004529.
- Han Z, Chen Q, Fu Z, Cheng S, Zhang X. Probiotic Spore-Based oral drug delivery system for enhancing pancreatic Cancer chemotherapy by Gut–Pancreas-Axis-Guided delivery. *Nano Lett.* 2022;22:8608–17.
- Wei G, et al. Nanozyme-Enhanced probiotic spores regulate the intestinal microenvironment for targeted acute gastroenteritis therapy. *Nano Lett.* 2024;24:2289–98.
- Song Q, et al. A probiotic Spore-Based oral autonomous nanoparticles generator for Cancer therapy. *Adv Mater.* 2019;31:e1903793.
- Song Q, et al. A bioinspired versatile spore coat nanomaterial for oral probiotics delivery. *Adv Funct Mater.* 2021;31:2104994.
- Chen Q, et al. Spore germinator-loaded polysaccharide microspheres ameliorate colonic inflammation and tumorigenesis through remodeling gut microenvironment. *Mater Today.* 2023;63:32–49.
- Chung CH, Jung W, Keum H, Kim TW, Jon S. Nanoparticles derived from the natural antioxidant, Rosmarinic acid, ameliorate acute inflammatory bowel disease. *ACS Nano.* 2020;14:6887–96.
- Huerta-Madroñal M, Caro-León J, Espinosa-Cano E, Aguilar MR, Vázquez-Lasa B. Chitosan – Rosmarinic acid conjugates with antioxidant, anti-inflammatory and photoprotective properties. *Carbohydr Polym.* 2021;273:118619.

37. Li J, Duan Q, Wei X, Wu J, Yang Q. Kidney-Targeted nanoparticles loaded with the natural antioxidant Rosmarinic acid for acute kidney injury treatment. *Small*. 2022;18:e2204388.
38. Lu B, et al. Rosmarinic acid nanomedicine for rheumatoid arthritis therapy: targeted RONS scavenging and macrophage repolarization. *J Control Release*. 2023;362:631–46.
39. Kundu B, Rajkhowa R, Kundu SC, Wang X. Silk fibroin biomaterials for tissue regenerations. *Adv Drug Deliv Rev*. 2013;65:457–70.
40. Farokhi M, Mottaghiab F, Reis RL, Ramakrishna S, Kundu SC. Functionalized silk fibroin nanofiber as drug carriers: advantages and challenges. *J Control Release*. 2020;321:324–47.
41. Tran HA, et al. Emerging silk fibroin materials and their applications: new functionality arising from innovations in silk crosslinking. *Mater Today*. 2023;65:244–59.
42. Kuwada T, et al. Identification of an Anti-Integrin  $\text{Av}\beta 6$  autoantibody in patients with ulcerative colitis. *Gastroenterology*. 2021;160:2383–e239421.
43. Cheng X, et al. Electrophoretic deposition of silk fibroin coatings with pre-defined architecture to facilitate precise control over drug delivery. *Bioact Mater*. 2021;6:4243–54.
44. Ma Y, et al. Oral nanotherapeutics based on *Antheraea pernyi* silk fibroin for synergistic treatment of ulcerative colitis. *Biomaterials*. 2022;282:121410.
45. Adebowale K, et al. Materials for cell surface engineering. *Adv Mater*. 2023;21:e2210059.
46. Lin S, et al. Surface-modified bacteria: synthesis, functionalization and biomedical applications. *Chem Soc Rev*. 2023;52:6617–43.
47. Xu C, Ban Q, Wang W, Hou J, Jiang Z. Novel nano-encapsulated probiotic agents: encapsulate materials, delivery, and encapsulation systems. *J Control Release*. 2022;349:184–205.
48. Hou W, et al. Decorating Bacteria with a therapeutic Nanocoating for synergistically enhanced biotherapy. *Small*. 2021;17:e2101810.
49. Li Q, et al. The progression of inorganic nanoparticles and natural products for inflammatory bowel disease. *J Nanobiotechnol*. 2024;22:17.
50. Kwon K, Jung J, Sahu A, Tae G. Nanoreactor for cascade reaction between SOD and CAT and its tissue regeneration effect. *J Control Release*. 2022;344:160–72.
51. Li G, et al. Optimizing the d-band center of Pd/CoPcS-Ti3C2Tx to enhance SOD/CAT-mimicking activities in the treatment of osteoarthritis. *Nano Today*. 2024;56:102250.
52. Li Y, Fu R, Duan Z, Zhu C, Fan D. Injectable hydrogel based on Defect-Rich multinanozymes for diabetic wound healing via an oxygen Self-Supplying cascade reaction. *Small*. 2022;18:e2200165.
53. Zhao S, et al. An orally administered CeO2@Montmorillonite nanozyme targets inflammation for inflammatory bowel disease therapy. *Adv Funct Mater*. 2020;30:2004692.
54. Liu J, et al. Biomaterials coating for on-demand bacteria delivery: selective release, adhesion, and detachment. *Nano Today*. 2021;41:101291.
55. Caruso R, Lo BC, Núñez G. Host-microbiota interactions in inflammatory bowel disease. *Nat Rev Immunol*. 2020;20:411–26.
56. Neurath MF, et al. Host-microbiota interactions in inflammatory bowel disease. *Nat Rev Gastroenterol Hepatol*. 2020;17:76–7.
57. Zhu Z, et al. Vanillin-based functionalization strategy to construct multifunctional microspheres for treating inflammation and regenerating intervertebral disc. *Bioact Mater*. 2023;28:167–82.
58. Li F, Long Y, Yu X, Tong Y, Gong L. Different immunoregulation roles of activin A compared with TGF- $\beta$ . *Front Immunol*. 2022;13:921366.
59. Lewis KA, et al. Betaglycan binds inhibin and can mediate functional antagonism of activin signalling. *Nature*. 2000;404:411–4.

#### Publisher's note

Springer Nature remains neutral with regard to jurisdictional claims in published maps and institutional affiliations.